Evidence of convective heat transfer enhancement induced by spinodal decomposition

P. Poesio,* A. M. Lezzi, and G. P. Beretta
Università di Brescia, Via Branze 38, 25123 Brescia, Italy
(Received 11 May 2006; revised manuscript received 25 January 2007; published 7 June 2007)

Spinodal decomposition can be driven by either diffusion or self-induced convection; the importance of convection relative to diffusion depends on the Péclet number, defined as the ratio between convective and diffusive mass fluxes. Diffusion is the dominating mechanism of phase segregation when the Péclet number is small—i.e., when viscosity and diffusivity are large—or when the domain characteristic size is small. For low-viscosity mixtures, convection is the dominating process and the segregation is very rapid as it takes a few seconds compared to the hours needed in the case of pure diffusion. In such cases, strong convective motion of the phase segregating domains is generated even in small-size systems and is almost independent of the temperature difference as long as it is below the transition value. We study experimentally the enhancement of heat transfer in a 1-mm-thick cell. A water-acetonitrile-toulene mixture is quenched into a two-phase region so as to induce convection-driven spinodal decomposition. The heat transfer rate is measured and compared to that obtained in the absence of convective motion. A substantial reduction in the cooling time obtains in the case of spinodal decomposition. The heat transfer enhancement induced by this self-induced, disordered but effectively convective effect may be exploited in the cooling or heating of small-scale systems whereby forced convection cannot be achieved because of the small sizes involved. A scaling analysis of the data based on the diffuse interface *H* model for a symmetric mixture near the equilibrium point yields very encouraging agreement and insights.

DOI: 10.1103/PhysRevE.75.066306 PACS number(s): 44.25.+f, 44.35.+c, 47.51.+a

I. INTRODUCTION

When an initially homogeneous (single-phase) mixture is cooled across its miscibility curve into the two-phase region, it phase separates either by nucleation or by spinodal decomposition. Nucleation is an activated process with a free energy barrier to overcome, as it occurs when the system is in an initially metastable equilibrium state. Spinodal decomposition, instead, denotes the relaxation to equilibrium of a system that is initially in an unstable equilibrium state, therefore with no energy barrier to overcome. While nucleation is a localized process that proceeds through the formation of nuclei that later grow and coalesce, spinodal decomposition is delocalized, as it occurs simultaneously over the entire domain. In this paper, we focus our attention on the spinodal decomposition of binary liquid mixtures with a convex miscibility curve (see Fig. 1).

The experimental results we present here are important for small-scale heat transfer enhancement applications. We show that vigorous convective motions are induced by spinodal phase separation in millimeter-size domains where forced convection is difficult to achieve.

It is noteworthy that during the review process of the present paper, a number of experimental and numerical works have appeared [1,2], showing a strong interest in spinodal decomposition-induced heat transfer enhancement due to its high potential applicability in miniaturized devices.

Experimentally, it has been shown that the phase segregation process following a temperature quench can be retarded either by quenching the mixture to a temperature T only a few millikelvin below the critical value T_{cr}—namely, to a reduced temperature $\tau=|T-T_{cr}|/T_{cr}<10^{-5}$ (see Refs. [3–5])—or by studying polymer blends with viscosity hundreds of times larger than that of water. In these cases, it was observed that, right after the system temperature crosses the miscibility curve, the initially homogeneous mixture starts to separate by diffusion only, leading to the formation of well-defined patches with near-equilibrium concentrations.

For simplicity, here we interpret the results by assuming local equilibrium conditions, but this hypothesis is now under debate [6]. In our case, the temperature itself is poorly defined, since we measure the temperature of a system far from stable equilibrium states (actually, passing through nonequilibrium states). Pragmatically, for the purpose of the present experimental study, we assume that the temperature is operationally defined by the reading of the electrical signal

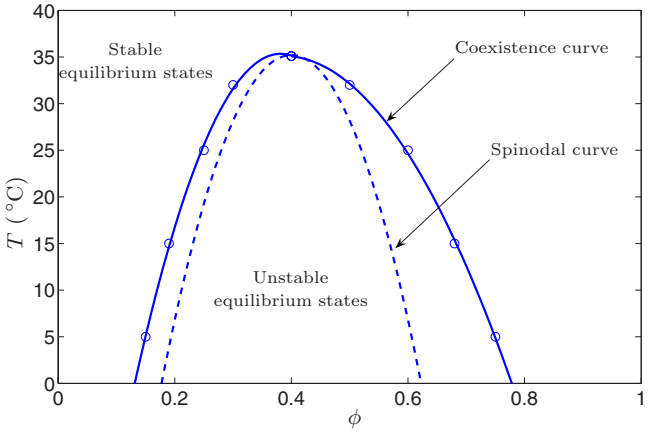

FIG. 1. (Color online) Phase diagram of a partially miscible binary mixture with upper critical solution temperature. The experimental points, taken from Ref. [11], are for water-toluene (phase 1, mole fraction ϕ) and acetonitrile (phase 2, mole fraction $1-\phi$).

*Electronic address: pietro.poesio@ing.unibs.it

out of the thermocouples. We are aware of the ongoing debate about the definition of a temperature for states far from stable equilibrium (see, for instance, Ref. [7] and references therein), but we leave such fundamental questions to further more detailed studies that are prompted by the present investigation.

The morphology of the mixture during spinodal decomposition depends on the composition of the system: for a critical mixture, the structure is bicontinuous and dendritic-like, while off-critical mixtures are characterized by droplike structures. In the so-called late stage of coarsening, the patches grow by diffusion and coalescence, until they become large enough that buoyancy dominates surface tension effects and the mixture separates by gravity. This occurs when the domains have sizes comparable to the capillary length $L_g=\sqrt{\sigma/g\Delta\rho}$, where σ is the surface tension, $\Delta\rho$ the density difference between the two phases at equilibrium, and g the gravitational acceleration. Typically, for the mixtures used in our experiments, the capillary length L_g is of $O(1\ \text{mm})$. This is in fact the case for highly viscous polymer blends, which need a long time to separate. On the other hand, liquid mixtures separate within seconds from quenching and therefore, in this case, diffusion is not the dominating mechanism of phase separation.

The other mechanism of segregation is convection-driven coalescence (see Ref. [8]), which implies that drops move against each other under the influence of nonequilibrium (square-gradient-type) capillary forces which develop at interfaces between domains with different compositions and, depending on their shape, effectively sum up to net forces that propel their bulk motions. This self-induced disordered bulk flow, predicted by the diffuse interface model (the so-called H model), has been observed experimentally [9]. It is much stronger in systems far from equilibrium—i.e., for deep quenching—when the composition of the drops and that of the surrounding phase are not equal to their equilibrium values [10]. Experimental evidence of the critical role of convection in phase segregation of deeply quenched liquid mixtures is reported in Ref. [11]. According to the scaling analysis in Ref. [8] the nonequilibrium body forces per unit volume scale as $F_\phi \sim 12\rho RT_{\text{cr}}\tau^2/LM_w$ confirming the strong dependence on the quench depth; here ρ is the density, R the gas constant, T_{cr} the mixture critical temperature, $\tau=(T_{\text{cr}}-T)/T_{\text{cr}}$ the quench depth, L the typical domain size, and M_w the mixture mean molecular mass.

The importance of convection relative to diffusion may be characterized by the mass Péclet number defined as the ratio between the convective and diffusive mass fluxes, $\text{Pe}=VL/D$, which scales [8] as $\text{Pe}\sim 24\rho RT_{\text{cr}}\ell^2\tau^3/\mu DM_w$, where V is a characteristic velocity of the bulk motions of the domains, D the molecular diffusivity, ℓ the typical interface thickness, and μ the fluid mixture viscosity: As the temperature changes during the quenching, also τ and Pe change during the process and therefore fluid domains, which initially move slowly, quickly accelerate during the process. According to Ref. [8] the characteristic velocity scales as $V\sim 24\rho RT_{\text{cr}}\ell^2\tau^3/\mu M_w L$.

At the end of the separation process, the interface between domains approaches equilibrium and the Péclet number may be linked to the equilibrium surface tension σ by the relation [8]

$$\text{Pe}\approx\frac{4\sigma\ell\tau}{\mu D}\approx\frac{2M_W\sigma^2}{3\mu D\rho RT_{cr}\tau}. \tag{1}$$

Therefore, in our experiments we compare different conditions based on the value of Pe computed at the end of the fast convective separating process.

Since it is known that convection is much more efficient in transporting scalar quantities, such as specific energy, in this paper we investigate the effect of spinodal-induced convective motions on the effective heat conductivity of the mixture. The aim of this paper is to provide experimental evidence that phase-change induced convection contributes to improve the heat transfer and that this is a consequence of the random mixing originating from the nonequilibrium capillary forces that result from nonlocal minimization of the free energy. We show that the heat and mass transfer problems are coupled and that by manipulating the mass transfer (i.e., the phase transition dynamics), we can control to some extent the heat transfer efficiency. Since the length scale characterizing spinodal decomposition is of the order of a few tenths of a micron, this method can be applied to small-scale devices and can be a very useful tool in the current rush towards miniaturization, since it may represent a heat transfer enhancement method applicable to cooling and heating in small-scale devices.

In Sec. II we describe the experimental setup and the procedure used for the investigation; in Sec. III, we analyze and discuss the experimental results. Conclusions are drawn in Sec. IV.

II. EXPERIMENTAL SETUP

An experimental setup was designed and built to visualize the phase separation process in the size range of 10 μm to 12 mm; a complete and detailed description of the setup can be found in Ref. [8]. It consists of a temperature-regulated quartz cell of 1 mm thickness and 8 mm $\times$45 mm sides. The quartz cell is flush-mounted on the top wall of a 6-mm-deep water channel that provides temperature control. A set of valves switches the water feed between a warm and a cold thermostat, thereby providing the quenching of the sample in the quartz cell. The recording is made by a high-speed, high-resolution, 8-bit digital camera equipped with a macrolens. The camera resolution is 1024 $\times$1024 pixels and the frame rate is set either to 75 fps or 125 fps. The smallest field of view is $1.6\times1.6\ \text{mm}^2$ with an optical resolution of 5 μm. The sample is back-lighted, using red light to enhance the contrast between the phases. The camera is set to an exposure time of 10 μs and is limited to a focal depth of 5 μm.

The temperature of the liquid mixture inside the cell is measured in the pragmatic sense specified in the Introduction by two 0.5-mm K-type thermocouples, with response time of 0.05 s. One thermocouple is placed in contact with the bottom of the cell (see Fig. 2), far away from the cooling stream; the other thermocouple is located in the bulk of the cell, 0.5 mm higher than the first one. Two K-type stainless-steel-sheeted 1.5-mm-o.d. thermocouples are placed in the cooling channel to monitor the temperature of the cooling

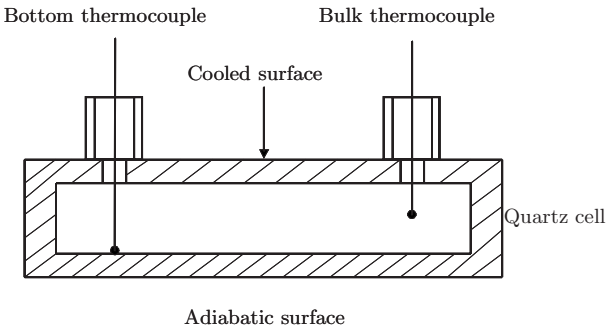

FIG. 2. Sketch of the experimental setup. A complete and detailed description can be found in Ref. [8].

water. All thermocouple acquisitions and the digital camera are triggered with the switching of the water feeding valves that starts the quenching. Measurements are gathered on a PC. An infrared camera was used to check if the temperature was uniform over the cell during the cooling-down transient. The results, not presented here, show a maximum temperature difference below 0.1 °C. This inhomogeneity is very small and difficult to reduce further.

The sample is a mixture composed of water, acetonitrile, and toluene with critical temperature at $T_{cr}=35$ °C. Thermodynamic properties are determined using the data given in Ref. [11]. The composition of the mixture used is 64% water, 35% acetonitrile, and 1% toluene; this mixture undergoes phase transition at 35 °C. Properties are reported in Table I. Acetonitrile and toluene are HPLC grade, while water is double-distilled. Crystal violet is added to the solution (50 ppm in weight) to facilitate the visualization since it dissolves preferentially in the organic-rich phase. When dissolved in such small amount as 50 ppm, crystal violet does not alter the phase diagram. Furthermore, it is a cationic emulsifier compound, which makes it ideal to study coalescence during the phase separation of liquid mixtures. For more details on the effects of surfactants on phase separation, see Ref. [11]. Being a critical mixture, a bicontinuous structure is expected during phase separation, as already reported in several publications. To change the Pe number, we change the fluid viscosity; the effect of viscosity on phase separation is reported in Ref. [8]. In order to modify the viscosity we add carbossimetilcellulose (CMC, CARBOFIX 5A type) to the solution. CMC is a water-soluble polymer, but it is completely in-soluble in the organic phase; we tested that CMC does not act as a modifier (at least up to 10% in weight) and, hence, it does not alter the coexistence curve; moreover, up to concentrations of 10%, water-CMC solutions show a Newtonian behavior. In all the experiments, we start with the

TABLE I. Properties of the critical mixture at equilibrium at 15 °C; from Ref. [11].

$\Delta\rho$	10	(kg/m^3)
μ	10^{-3}	(Pa s)
σ	10^{-2}	(N/m)
D	10^{-9}	(m^2/s)

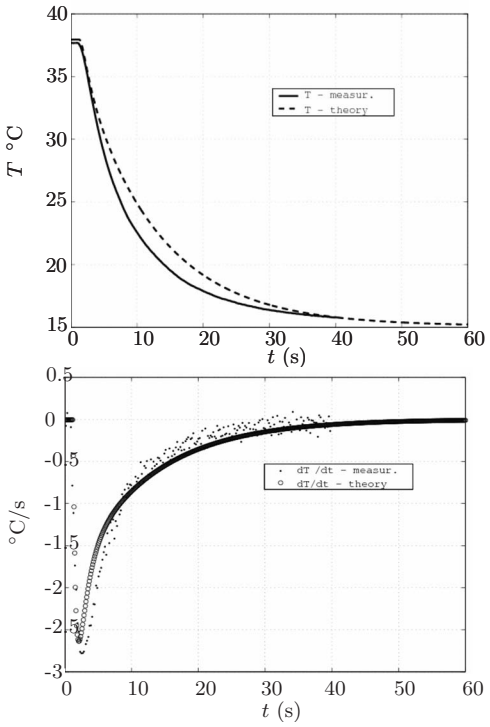

FIG. 3. Reference comparisons between measurements and theoretical one-dimensional conduction prediction when the cell is filled with pure water.

mixture in its phase-separated state at a constant temperature of 20 °C. The mixture is first heated to 38 °C, then mixed thoroughly, and, eventually, quenched back below its critical point. Mixing the solution before quenching is extremely important as we want to study the behavior of an initially homogeneous mixture. As shown in Ref. [9], when the separated phases are heated at 38 °C, but not mixed, after 2 h, the mixture is still mostly demixed, except for a very thin, few-millimeters-thick, layer where a sharp concentration gradient is present.

Quenching is obtained by switching the valves so that cold water enters the channel that cools the top surface of the quartz cell. The bottom surface is in contact with air at room temperature and on the time scale of the phenomenon can be assumed adiabatic. Note that in our setup the cooling starts at the top of the cell while the bottom is at a higher temperature, so one may wonder whether a thermal instability occurs and if thermal natural convection appears. The onset of such instability occurs at a critical Rayleigh number Ra$\sim$1700 while in our case Ra is of $O(10)$, far below the critical value.

III. RESULTS

First we analyze in detail a typical experiment and then we present some macroscopic results on cooling time during the linear isotropic domain growth stage.

In Fig. 3, we plot the reading out of the thermocouples as a function of time at two locations inside a cell filled with pure water. As shown in Fig. 2, one thermocouple is placed at the bottom of the cell wall and the other at a position

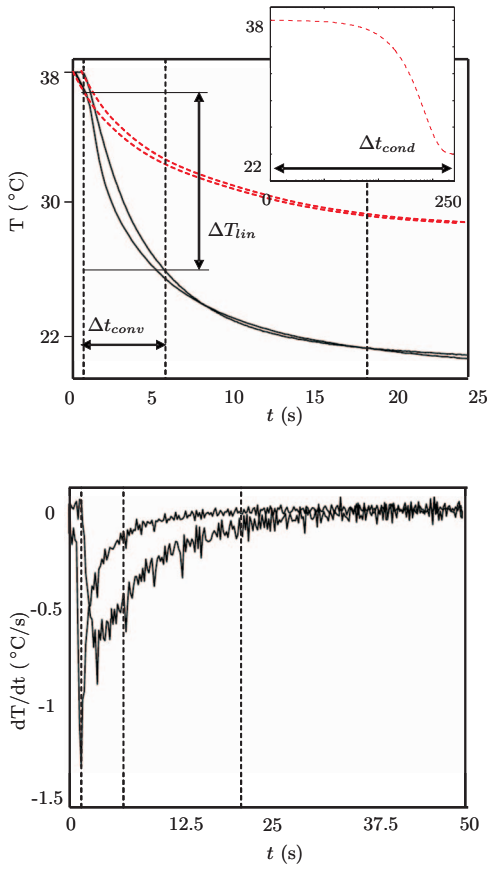

FIG. 4. (Color online) Top graph: thermocouple readings at two locations inside the cell. The red dashed line represents the evolution of the temperature calculated by a one-dimensional model in the bulk of the cell, assuming pure conduction and mean mixture properties. Bottom graph: rates of change of the thermocouples readings at two locations inside the cell. Vertical dashed lines separate the four typical stages of the process (see text and Fig. 5).

0.5 mm higher from the bottom. In the following, we refer to these readings as *temperatures* even if this term may not be the most appropriate as discussed in the Introduction. On the same graph in Fig. 3, we also report the temperature as calculated assuming a pure one-dimensional conduction problem. The two water channels (from which the thermocouples are inserted; see Fig. 2) have an effect on the temperature field and, hence, on the temperatures recorded by the thermocouples; however, as we could see from numerical investigations based on the commercial code FLUENT, this effect is small and the one-dimensional assumption is valid. The convective heat transfer coefficients assumed in the pure conduction theoretical computation are tuned by comparing the numerical results against the experimental ones in the reference case of a cell filled with water only. As shown in Fig. 3, the comparison is rather good both concerning the temperature evolution and the cooling rate. The convective heat transfer coefficients found by this procedure are used in the following to compute the temperature evolution inside the cell filled with the partially miscible mixture.

Figure 4 shows the typical cooling curve obtained when the cell is filled with the test mixture. The dashed curve represents a theoretical one-dimensional computation of the temperature evolution in the bulk of the cell assuming the averaged properties. At $t=0$, the cooling process starts; the temperature is above the critical value and separation has not started yet. The thermocouple in the bulk of the cell records a lower temperature than that placed 0.5 mm below, in contact with the adiabatic wall (Fig. 2). In this period, the heat transfer is conduction dominated. Figure 4 shows also the comparison between the cooling rate at the two thermocouple locations. During the second period (from $t=1.2$ s to $t=6.4$ s), mass transfer is driven by convection, as previously noted in Ref. [8]; domains grow and move isotropically throughout the cell. These self-induced disordered bulk motions are at the origin of the heat transfer enhancement, and the cooling time is substantially reduced compared to the case of pure conduction—dashed curve; the temperature difference between the two thermocouples decreases (see Fig. 4), indicating a mixing process due to fluid domains moving around in all directions and, hence, also in the vertical one. During their motion, domains grow and become heavier, so gravity effects start playing a role: the heavier phase sinks while the lighter floats. The motion is not isotropic anymore, but there is a net vertical movement that has the effect to make the temperature field uniform. During this stage, there is no difference between the temperatures recorded by the two thermocouples, indicating a convective dominated process. The cooling rate at the lower thermocouple is larger than the one at the center, and also in this case comparison with the pure conduction problem indicates that the process is much faster. The comparison between the theoretical curve and the experimental ones clearly demonstrates the enhancement of the heat transfer as a consequence of the motions induced by spinodal phase transition. At about 20 s after the beginning of the quenching, the temperature is uniform within the cell and its value is different from the final one by only fractions of a degree; in the case of pure conduction it would take much longer to cool down completely: after 20 s the cooling by conduction is far from being completed. Since spinodal decomposition occurs simultaneously over the entire domain (being a delocalized process), the mixing is very efficient and that explains why the cooling time is drastically reduced compared to pure diffusion.

From a qualitative point of view, all the experiments we carried out show a similar behavior and there are four different stages, Fig. 5: (i) initial conduction, necessary to drive the system at the transition temperature; (ii) isotropic convection, during which the domains move randomly and isotropically through the cell; (iii) gravity-dominated convection during which the domains move preferentially under the influence of gravity; (iv) conduction when the mixture is fully separated.

During the phase separation process, the fluid domains enlarge and, hence, the characteristic length increases. In Fig. 6, we show the evolution of the characteristic length during the isotropic convective stage for three different experiments. The length scale reported here is computed as the first moment of the structure factor; the structure factor is defined in Ref. [12] and it accounts for the size distribution of the domains over the observation area. An example of the structure factors computed at different instants is shown in Fig. 7; when properly scaled, the structure factors do collapse on a

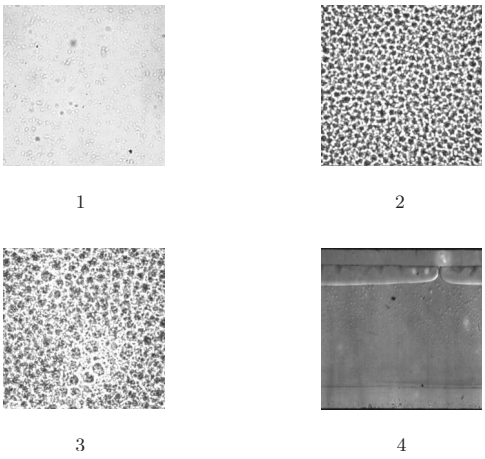

FIG. 5. Typical morphology during each stage. The first three frames are taken in a horizontal plane; the fourth one is taken in a vertical plane to show segregation due to gravity.

common master curve (see Ref. [8]). During the isotropic convective stage, the typical size increases linearly with time as ascribed by a convection-dominated phase separation mechanism; it is also worth noting that the characteristic length scale is larger than the crossover length computed following Refs. [13,14]—i.e., $L_c \approx 10$ μm. The typical velocity, estimated by visual inspection of the high-speed recorded movies, is of the order of 1 mm/s, much smaller than the predicted values in Ref. [13], but in agreement with other experimental observations (see Ref. [15]). During the third stage (gravity-dominated convection), we could not find a procedure to mathematically estimate the length scale. Referring to the experiments reported in Fig. 4, from a visual inspection we could see a dimension of about 100 μm at the beginning (T=25 °C), a dimension of about 400–500 μm in the middle (T=23 °C), and a dimension of 800–1000 μm at the end (T=21 °C). The corresponding velocities, again estimated by visual inspection, are, respectively, 1 mm/s, 5 mm/s, and 0.1 mm/s. At the end of the third stage, convection is not important anymore; the fluid domains slow down and diffusion takes over becoming the dominant mechanism.

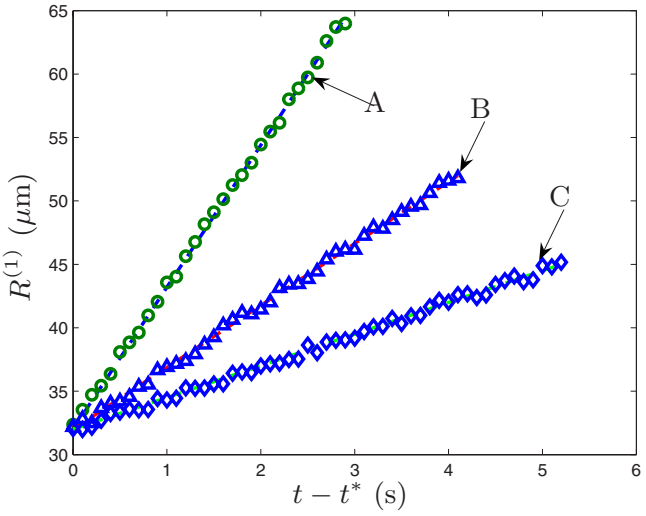

FIG. 6. (Color online) Evolution of the domain size corresponding to three different experimental situations. A: τ=0.067. B: τ=0.045. C: τ=0.017. t^* indicates the initial instant of the convection-dominated stage. Experiment B is relative to Fig. 4.

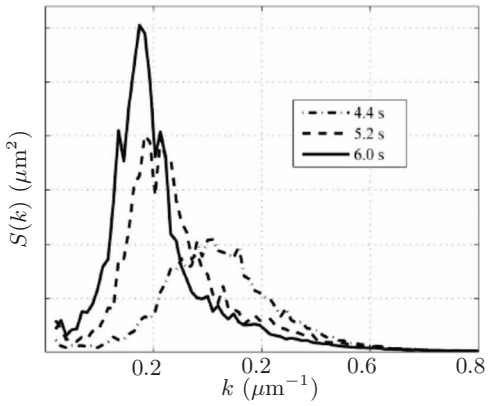

FIG. 7. Structure factor computed at different instants within the linear isotropic convection-dominated stage. These structure factors are relative to the experiment shown in Fig. 4; k indicates the wavelength associated with the domain size by the relation $k=2\pi/R$.

So far, we have qualitatively analyzed the cooling process during spinodal decomposition. We try here a more quantitative analysis of the so-called linear isotropic stage. In Ref. [8], a number of relations have been derived that are valid during this stage and we want to make use of them to link in a quantitative way the mass transfer process to the heat transfer.

To evaluate the effect of spinodal-induced convective heat transfer, we compare the time needed for the system to lower its temperature in the case of pure conduction with the time needed if convection is present as well. During the linear isotropic growth stage, the system temperature drop is of ΔT_{lin} (see Fig. 4). During this stage, the mass transfer is convection dominated and we call the time interval Δt_{conv}. Then, we compute the time interval Δt_{cond} needed for the system to undergo the same quenching ΔT_{lin} when mass diffusion is the only mechanism.

For each experiment, we compute the typical domain size evolution by means of the structure factor; when the evolution of the typical domain size is known, we look for the linear part (see Fig. 6). The temperatures at the beginning (T^i_{lin}) and at the end (T^f_{lin}) of the linear isotropic growth period are known (and $\Delta T_{lin}=T^i_{lin}-T^f_{lin}$ can be computed) as well as the duration of this stage, formally defined as $\Delta t_{conv}=t(T^f_{lin})-t(T^i_{lin})$.

We run then a pure conduction simulation with the initial temperature set at T^i_{lin} and boundary conditions identical to the experimental. The computation is run up to the instant when the temperature equals T^f_{lin}, so as to compute the time interval Δt_{cond}.

Figures 8 and 9 represent two completely independent data sets: the data set in Fig. 8 is obtained by keeping the same mixture properties and changing the quenching depth τ. For further analysis, we find it convenient to define a partial quenching depth τ_{lin} as

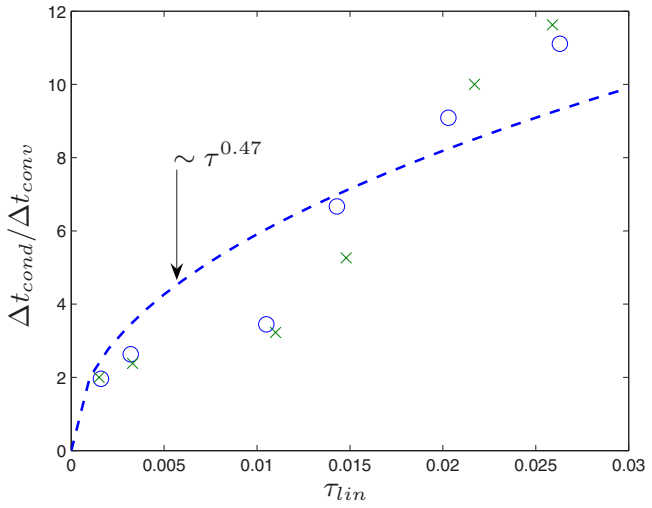

FIG. 8. (Color online) Effective heat transfer enhancement factor as a function of quenching depth. Data $A-N$ in Table II.

$$\tau_{lin} = \frac{T_{cr} - T_{lin}^{f}}{T_{cr}}, \tag{2}$$

where T_{lin}^{f} is the temperature at the end of the linear stage. All the data plotted in Figs. 8 and 9 are summarized in Table II. The data set in Fig. 9 is obtained by changing the mixture viscosity; however, for this data set there are variations in τ_{lin} as well (see Table II).

We now attempt to correlate all the experiments using the ratio $\Delta t_{cond}/\Delta t_{conv}$ which represents an effective heat transfer enhancement factor or its inverse which is a dimensionless cooling time.

Figure 8 shows that the effective enhancement increases with the quenching depth τ_{lin} since convective motions become more vigorous; this conclusion is supported by the analysis of the driving force F_{ϕ} that scales with the instantaneous quenching depth τ—more precisely, $F_{\phi} \sim \tau^2$ [8].

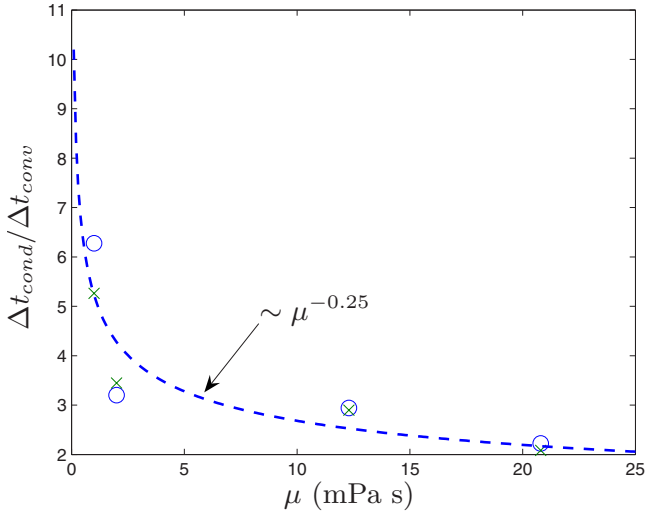

FIG. 9. (Color online) Effective heat transfer enhancement factor as a function of viscosity. Data $O-V$ in Table II.

These data for the ratio $\Delta t_{cond}/\Delta t_{conv}$ are fitted by the power law

$$\frac{\Delta t_{cond}}{\Delta t_{conv}} \sim \tau_{lin}^{0.47}. \tag{3}$$

The second data set is plotted in Fig. 9 where the enhancement factor $\Delta t_{cond}/\Delta t_{conv}$ is shown to be a decreasing function of viscosity (fluid viscosity μ is changed by the addition of CMC, a water-soluble polymer that does not alter the mixture properties except for the value of viscosity). These data are fitted by the power law

$$\frac{\Delta t_{cond}}{\Delta t_{conv}} \sim \mu^{-0.25}. \tag{4}$$

Expectedly, as viscosity increases (and hence the mass transfer is slowed down) the domain mobility decreases and the convective motions weaken, leading to a less vigorous heat transfer: the mass process is still convection driven, but it is less vigorous.

A joint curve fitting of the data sets in Figs. 8 and 9 yields

$$\frac{\Delta t_{cond}}{\Delta t_{conv}} \sim 9.9 \frac{\tau_{lin}^{0.44}}{\mu^{0.23}}; \tag{5}$$

note that the exponents in Eq. (5) are very close to the ones found in the independent fittings in Eqs. (3) and (4).

Since the thermal and mass diffusivities may be assumed to be constant in our experiments, a linear relation between Pe_T and Pe is expected:

$$\frac{\mathrm{Pe}_T}{\mathrm{Pe}} = \frac{VL}{\alpha}\frac{D}{VL} = \frac{D}{\alpha} = \mathrm{Le}, \tag{6}$$

where we assume the same characteristic velocity V and the same typical length L for both Péclet numbers, because the thermal convection is a direct consequence of the mass convection, and we recall that the ratio of mass and thermal diffusivity is the Lewis number (Le), which for a 65%-water–35%-acetonitrile mixture is of order 0.1. Combining Eq. (6) with Eq. (B9) of Ref. [8], derived from the diffuse-interface H model for a symmetric mixture near the critical point, we obtain the following scaling relations for the thermal Péclet number:

$$\mathrm{Pe}_T \approx \frac{12\rho R T_{cr} \tau_{lin}^2 a^2}{\mu\alpha M_W} \approx \frac{2M_W\sigma^2}{3\mu\alpha\rho R T_{cr}\tau_{lin}} \approx \frac{288\rho R T_{cr} D^2 \tau_{lin}^6}{\mu\alpha M_W (dL/dt)^2}, \tag{7}$$

where a is the typical length of spatial inhomogeneities that appear in the square-gradient term of the generalized Cahn-Hillard free energy,

$$\tilde{g} = g_0 + \frac{1}{2}RTa^2(\nabla\phi)^2, \tag{8}$$

with g_0 the free energy of the uniform (binary) mixture at equilibrium and ϕ the mole fraction of one of the (two) components. We denote by dL/dt the growth rate of the domain size during the isotropic convective stage of the separation process, before the onset of the buoyancy effects. Re-

TABLE II. Summary of the experimental results. Sequence $G-N$ is a repetition of the same experimental conditions as for sequence $A-F$. Sequence $S-V$ is a repetition of sequence $O-R$.

Experiment	τ	μ (mPa s)	τ_{lin}, Eq. (2)	$\frac{\Delta t_{conv}}{\Delta t_{cond}}$	$\frac{dL}{dt}$, Eq. (12) (μm/s)	$\dot{R}^{(1)}$, Ref. [8] (μm/s)	σ Eq. (11) mN/m	$a\times 10^{-8}$, Eq. (10) (m)
A	0.0065	1.0	0.0016	1.96	0.07	0.06	2.27	1.7
B	0.0097	1.0	0.0032	2.63	0.47	0.45	3.96	2.2
C	0.0325	1.0	0.0105	3.34	11.22	12.17	10.1	3.3
D	0.0487	1.0	0.0143	6.67	26.14	27.35	13.0	3.7
E	0.0811	1.0	0.0203	9.09	66.90	64.90	17.1	4.2
F	0.0974	1.0	0.0263	11.10	135.20	116.7	21.1	4.6
G	0.0065	1.0	0.0015	2.00	0.067	0.06	2.27	1.7
H	0.0097	1.0	0.0033	2.38	0.414	0.39	3.96	2.2
I	0.0325	1.0	0.0110	3.22	10.03	10.52	10.1	3.3
L	0.0487	1.0	0.0148	5.26	29.98	26.63	13.0	3.7
M	0.0811	1.0	0.0217	10.00	67.27	71.08	17.1	4.2
N	0.0974	1.0	0.0259	11.62	118.74	118.2	21.1	4.6
O	0.0325	1.0	0.0105	6.28	7.80	7.18	10.1	3.3
P	0.0325	2.0	0.0108	3.20	8.30	8.18	11.9	4.3
Q	0.0325	12.3	0.0123	2.94	10.33	11.7	18.5	8.6
R	0.0325	20.8	0.0159	2.22	11.22	9.8	21.0	10.5
S	0.0325	1.0	0.0110	5.26	7.98	7.85	10.3	3.6
T	0.0325	2.0	0.0130	3.44	7.47	8.18	12.4	4.8
U	0.0325	12.3	0.0145	2.90	11.71	10.94	19.7	9.2
V	0.0325	20.8	0.0165	2.08	11.54	10.6	22.1	11.4

lation (7) is valid only during the linear isotropic growth period.

Furthermore, the ratio $\Delta t_{cond}/\Delta t_{conv}$ can be interpreted as the thermal Péclet number Pe_T characterizing the thermal problem and it can be seen as the ratio between the thermal diffusion characteristic time and the convection characteristic time—i.e., $\mathrm{Pe}_T = VL^2/\alpha L$, where $\Delta t_{cond} \sim L^2/\alpha$ (α being the thermal diffusivity) and $\Delta t_{conv} \sim L/V$. Interpreting the ratio $\Delta t_{cond}/\Delta t_{conv}$ as the thermal Pe_T, the result in Eq. (5) yields the estimate

$$Pe_T \sim 9.9 \frac{\tau_{lin}^{0.44}}{\mu^{0.23}}. \tag{9}$$

Equation (9) and the corresponding experimental data are reported in Fig. 10.

We now combine this empirical result with the scaling reported in Eq. (7) valid within the diffuse interface H model for a symmetrical mixture near the critical point and obtain the following order-of-magnitude estimates:

$$a \approx \left(\frac{\mathrm{Pe}_T \mu \alpha M_W}{12 \rho R T_{cr} \tau_{lin}^2} \right)^{1/2} \sim 8.6 \times 10^{-9} \tau_{lin}^{-0.78} \mu^{0.385}, \tag{10}$$

$$\sigma \approx \left(\frac{\mathrm{Pe}_T 3 \mu \alpha \rho R T_{cr} \tau_{lin}}{2 M_W} \right)^{1/2} \sim 4.12 \tau_{lin}^{0.72} \mu^{0.385}; \tag{11}$$

$$\frac{dL}{dt} \approx \left(\frac{288 \rho R T_{cr} D^2 \tau_{lin}^6}{\mathrm{Pe}_T \mu \alpha M_W} \right)^{1/2} \sim 12.9 \tau_{lin}^{2.78} \mu^{-0.385}, \tag{12}$$

where the dimensional constants on the right-hand side are obtained assuming $R=8.3$ kJ/(kmol K), $T_{cr}=308$ K, ρ

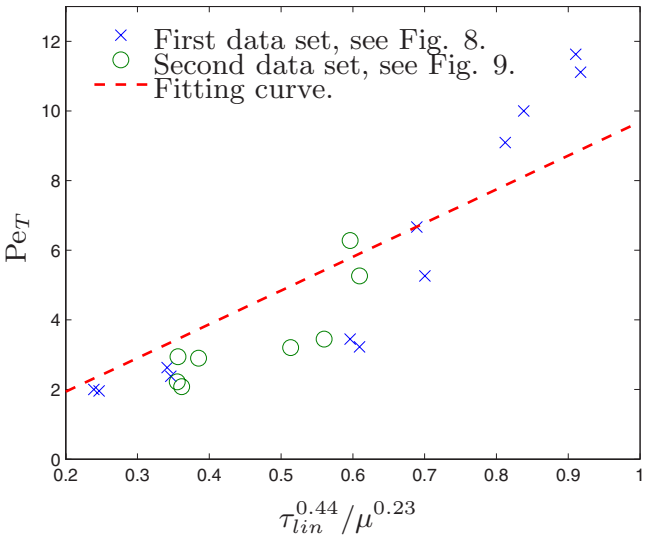

FIG. 10. (Color online) Circles and crosses represent the experimental values of both data sets. The dashed line is the fitting curve, Eq. (9).

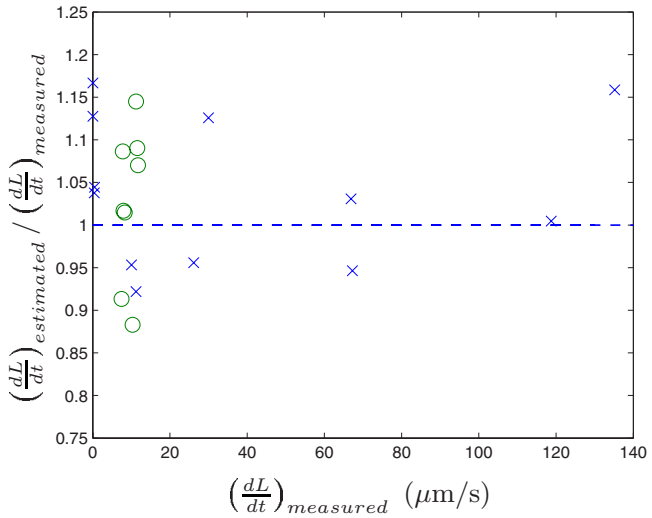

FIG. 11. (Color online) Comparison between measured domain growth rate $(dL/dt)_{measured}$ with the estimated value $(dL/dt)_{estimated}$ obtained from Eq. (12). More precisely, $(dL/dt)_{measured}=\dot{R}^{(1)}$, where $R^{(1)}$ is computed as the first moment of the structure factor, Ref. [8].

$=10^3$ kg/m^3, $\alpha=10^{-8}$ m^2/s, $D=10^{-9}$ m^2/s, and $M_W=22.6$ kg/kmol, where μ is in Ns/m^2, τ_{lin} is dimensionless, a is in m, σ is in N/m, and dL/dt is in m/s. Since the interface width ℓ can be computed from Eq. (10) by the relation $\ell=a/\sqrt{\Psi-2}$ and since near the critical point the Margules parameter Ψ scales as $\Psi-2\approx 2\tau$, it can be concluded that as $\tau\to 0$ the interface width $\ell\to\infty$, in agreement with the fact that at the critical point, the interface width is very large. Furthermore, a is estimated to be of the order 10^{-8} m (see Table II), in close agreement with independent estimates—Ref. [15]—in the range 10^{-8}–10^{-7} m.

The surface tension is estimated to be in the order of 10^{-2} N/m, which is a reasonable value for liquid-liquid mixtures, and, in addition to that, as τ_{lin} increases, and hence, the final temperature decreases, the surface tension σ increases as normally expected (see Ref. [16]).

Finally, since dL/dt can be estimated from Eq. (12) and since it can also be measured independently from image analysis [8], we can evaluate the goodness of the scaling procedure by comparing the estimated values to the measured ones. This comparison is carried out in Fig. 11; as can be seen, the agreement between measurements and estimated values is within ±20%. The agreement is excellent in spite of several gross approximations, such as (i) the assumption that all the thermophysical properties are temperature independent; (ii) the identification of a mean domain size growth rate, given as the first moment of the structure factor $R^{(1)}$, with an order of magnitude estimate for the growth rate of a *typical* domain size L; (iii) the adoption, in the scaling analysis, of τ_{lin} as an estimate of τ, assumed constant during the linear growth interval even though the temperature is changing [8]; (iv) the experimental uncertainties: the largest disagreement is at small value of dL/dt where experimental errors have a larger impact.

In agreement with some previous results [8], $\dot{R}^{(1)}$ is only slightly dependent on the viscosity [Table II and Eq. (12)] as expected for a bicontinuous morphology of a critical mixture.

Even if there are some discrepancies between the estimated domain growth rates and the measured ones, we find the results of our scaling analysis very encouraging. In particular, the analysis seems to confirm indirectly the assumed relation (6) between Pe_T and Pe, which is based on the assumption of the same characteristic scales L and V for both the mass and the heat transfer mechanisms, at least during the constant-growth-rate stage.

IV. CONCLUSIONS

We present experimental data on spinodal decomposition with particular emphasis on the coupling between the heat and the mass transfer processes. We show that the convective motion generated by nonequilibrium capillary forces during spinodal decomposition results in a heat transfer enhancement. The coupling is clearly demonstrated by the observed relation between Pe_T and Pe. Our scaling analysis gives some indications that the Pe_T scales as $\tau^{0.44}/\mu^{0.23}$, but more detailed theoretical analysis is needed in order to understand the scaling of the Péclet numbers.

A reason why spinodal decomposition is so efficient in mixing (momentum, species, and internal energy) is related to the fact it occurs simultaneously over the entire region, as opposed to nucleation, which appears only at few spots. Differently from other phase-change processes, the mixture can be properly targeted for a specific application in order to achieve the desired effect. By changing the amount of toluene, which acts as a modifier, the coexistence curve can be shifted up or down and the influence of the different stages can be changed; furthermore, the position of the coexistence curve can be calibrated according to the operating temperatures. For a given composition, the cooling rate can be slowed down by adding a viscosifier (such as CMC) that decreases the Pe number and, hence, the thermal Pe_T. It is worth noting that the proposed system is particularly suitable in small-scale devices, where vigorous convective cooling can be a difficult task to achieve. So this preliminary study can prompt further analysis aiming at investigating spinodal phase transition to enhance heat transfer, as already attempted by some authors recently [2,15] during the review of the present work.

The scheme reported here—cooling of a closed cell—may not be the most useful from the application viewpoint. Indeed, this paper is just a first step aimed at proving the principle that we may achieve important heat transfer enhancement and control capability in small-size devices by exploiting the disordered convection generated by the square-gradient capillary forces that characterize spinodal decomposition. Encouraged by the evidence reported in the present study, we have designed and manufactured a compact heat exchanger (shell and tube type) based on the mechanism just discussed. Experimental results will be reported elsewhere.

[1] D. Molin and R. Mauri, Flow Sci. Technol. (to be published).
[2] S. Gat, A. Ullmann, and N. Brauner (unpublished).
[3] Y. C. Chou and W. I. Goldburg, Phys. Rev. A **20**, 2105 (1979).
[4] P. Guenoun, R. Gastaud, F. Porrot, and D. Beysens, Phys. Rev. A **36**, 4876 (1987).
[5] N. C. Wong and C. Kmnobler, Phys. Rev. A **24**, 3205 (1981).
[6] H. Tanaka, Phys. Rev. E **51**, 1313 (1995).
[7] J. Casas-Vazquez and D. Jou, Rep. Prog. Phys. **66**, 1937 (2003).
[8] P. Poesio, G. Cominardi, A. M. Lezzi, R. Mauri, and G. P. Beretta, Phys. Rev. E **74**, 011507 (2006).
[9] G. Santonicola, R. Mauri, and R. Shinnar, Ind. Eng. Chem. Res. **40**, 2004 (2001).
[10] N. Vladimirova, A. Malagoli, and R. Mauri, Phys. Rev. E **60**, 6968 (2000).
[11] R. Gupta, R. Mauri, and R. Shinnar, Ind. Eng. Chem. Res. **38**, 2418 (1999).
[12] V. M. Kendon, M. E. Cates, I. P. J.-C. Desplat, and P. Bladon, J. Fluid Mech. **440**, 147 (2001).
[13] H. Furakawa, Phys. Rev. A **31**, 1103 (1985).
[14] E. D. Siggia, Phys. Rev. A **20**, 595 (1979).
[15] R. Mauri, F. Califano, E. Calvi, R. Gupta, and R. Shinnar, J. Chem. Phys. **118**, 8841 (2003).
[16] D. Tabor, *Gases, Liquids, and Solids*, 3rd ed. (Cambridge University Press, Cambridge, England, 1993).